An X-ray absorption spectroscopy study of argutite solubility and aqueous Ge(IV) speciation in hydrothermal fluids to 500 degrees C and 400 bar

Gleb S. Pokrovski, Jacques Roux, Jean-Louis Hazemann, Denis Testemale

HAL Id: hal-00714435
https://hal.science/hal-00714435

Submitted on 4 Jul 2012

An X-ray absorption spectroscopy study of argutite solubility and aqueous Ge(IV) speciation in hydrothermal fluids to 500°C and 400 bar

Gleb S. Pokrovski,[1,*] Jacques Roux,[2] Jean-Louis Hazemann,[3] & Denis Testemale[3]

1- Experimental Geochemistry & Biogeochemistry Group, Laboratoire des Mécanismes et Transferts en Géologie (LMTG, UMR 5563 of CNRS), 14 avenue Edouard Belin, 31400 Toulouse, France
2- IPGP/CNRS, UMR 7047, 4 Place Jussieu, 75252 Paris, cedex 05, France
3- Laboratoire de Cristallographie (CNRS) & SNBL/ESRF, 6 rue Jules Horowitz, B.P. 220, 38043 Grenoble, France

* *Corresponding author*:
phone: (33)-(0)5-61-33-26-18; fax: (33)-(0)5-61-33-25-60; e-mail: *pokrovsk@lmtg.obs-mip.fr*

_____

Abstract: Dissolution of synthetic argutite (GeO$_2$, tetragonal, rutile-like) in pure water, and local atomic structure around Ge(IV) in aqueous solution were characterized by *in situ* X-ray Absorption Fine Structure (XAFS) spectroscopy at the Ge K-edge using a new high temperature - high pressure cell. XAFS transmission and fluorescence spectra were collected from germanic acid aqueous solutions of 0.02 to 0.09 mol Ge/kg H$_2$O at ambient pressure and temperature, and from a 0.04 mol Ge/kg H$_2$O solution at 400 bar from 20 to 450°C. Spectra at all temperatures and concentrations exhibit the 1st shell contribution from 4±0.3 oxygen atoms at 1.75±0.01Å, consistent with a tetrahedral structure of the Ge(OH)$_4$ complex which is a chemical analog of Si(OH)$_4$ and is the dominant Ge aqueous species, in agreement with previous solubility and potentiometric measurements. The constancy of Ge(OH)$_4$ structural parameters over the wide temperature and fluid-density range is consistent with the strong covalent character of the Ge-(OH) bonds. A dissolution experiment on argitite in pure H$_2$O was carried out at 400 bar from 200 to 500°C by monitoring the height of the Ge absorption edge of transmission spectra. The solubility of GeO$_2$, derived from a classical X-ray absorption relation using the absorption height values and fluid density, increases with increasing temperature up to 400°C but decreases at 450 and 500°C, similar to that observed for quartz. The new solubility data were analyzed using both a density model and the revised HKF equation of state to better constrain Ge(OH)$_4$ thermodynamic properties. Calculations using these models indicate that despite strong similarities in the structure and energetics of aqueous germanic acid and silica, differences in the thermodynamic properties of germanate and silicate dissolution reactions may account for the increase of the Ge/Si ratio observed in high temperature natural fluids.

Keywords: germanium; X-ray Absorption Fine Structure (XAFS) spectroscopy; argutite; solubility; Ge hydroxide complexes; density model; HKF model; Ge/Si ratio

1. Introduction

Although in the Earth's crust most germanium is dispersed through silicate minerals due to the isomorphic substitution of Ge(IV) to the chemically similar Si(IV), germanium can be highly enriched relative to silicon in a variety of geological materials such as secondary clay minerals, sulfides, iron hydroxides, coals, and hydrothermal fluids (e.g., Bernstein, 1985; Bernstein & Waychunas, 1987). This property makes germanium a potentially useful geochemical tracer of continental weathering intensity, hydrothermal and tectonic activity, or fluid sources (e.g., Froelich et al., 1985; Murnane & Stallard, 1990; Kurtz et al., 2002). For example, the Ge/Si atomic ratio is ~0.6×10^{-6} in rivers, $(1 \text{ to } 3) \times 10^{-6}$ in most silicate minerals, and $(10 \text{ to } 100) \times 10^{-6}$ in high-temperature hydrothermal fluids (Froelich et al., 1985; Kurtz et al., 2002; refs therein). It is likely that such significant variations may be related to differences in aqueous speciation and/or crystal chemistry between Ge and Si. For example, it has been recently suggested that possible differences in the thermodynamic properties between Ge and Si aqueous complexes and minerals at elevated temperatures could explain the anomalously high Ge/Si ratios observed in hot natural fluids emanating from mid-ocean ridges (Pokrovski & Schott, 1998a). Thus, knowledge of Ge aqueous complexes stability (i.e., thermodynamics), structure, and Ge coordination is of importance for the quantitative use of the Ge/Si ratios to trace natural processes. At present, however, the scarcity of such information, particularly at elevated temperatures, greatly hampers the quantitative prediction of both Ge/Si ratios in hydrothermal/magmatic processes and Ge-versus-Si hydrothermal fluxes to the hydrosphere and biosphere.

Previous studies have shown that the easiness of Ge, contrary to Si, to extend its coordination from 4 to 6, is responsible for the preferential incorporation of Ge into iron hydroxide minerals (Bernstein & Waychunas, 1987), and aqueous chelate complexes with organic ligands (Pokrovski & Schott, 1998b; Pokrovski et al., 2000). Nevertheless, in most of low to moderate temperature organic-poor superficial and hydrothermal waters, germanium, like

silicon, is present as the neutral hydroxide complex, germanic acid, of the presumed stoichiometry $Ge(OH)_4$ based on the analogy with silicic acid. The knowledge of the thermodynamic properties of this species is, however, limited to 350°C (Pokrovski & Schott, 1998a), and its exact structure and coordination are not known at temperatures above ambient. The aim of the present study is to provide new data about Ge species structure and stability in near and supercritical aqueous fluids using X-ray Absorption Spectroscopy.

Until recently, most of measurements of mineral solubilities in high-temperature/pressure (T-P) aqueous fluids are performed using batch or flow reactors which require fluid quenching after or sampling during the experiment. Thus, significant efforts are necessary to account for or avoid possible precipitation/adsorption or oxidation (depending on the chemical system) of the initial high T-P fluid during sampling or quenching procedures. To obtain species identities and stoichiometries from the measured total dissolved metal concentrations, one requires many experimental points and an accurate knowledge of the intensive parameters (e.g., pH, Eh, ligand activities) which are often poorly constrained at elevated temperatures and pressures. In the recent years, the development of high T-P spectroscopic cells (e.g., Bassett et al., 2000; Hoffmann et al., 2000) and improvement of laser and X-ray sensitivities allowed the use of vibrational (Raman, UV) and X-ray Absorption spectroscopies for numerous *in situ* investigations of metal speciation in a variety of systems in hydrothermal fluids, most of them limited to temperatures up to ~350°C (see Brown & Sturchio, 2002 for a review). A few studies of mineral solubilities by X-ray fluorescence and Raman scattering using diamond-anvil techniques allowing measurements to 10's kbar have recently appeared (e.g., quartz, Zotov & Keppler, 2002; AgCl, Schmidt & Rickers, 2003; $SrCO_3$, Sanchez-Valle et al., 2003). However, a simultaneous *in situ* measurement of both species structures and mineral solubilities at near- and supercritical conditions in a single series of experiments or using a single cell configuration still remains rare.

X-ray Absorption Fine Structure (XAFS) spectroscopy provides in fact a very efficient, and, sometimes, unique way of both *in situ* determination of metal local structure in its complexes, and solid phase solubilities (aqueous concentrations). In this study, we used a new X-ray cell allowing simultaneous acquisition of transmission and fluorescence spectra at high temperature and pressure to measure both Ge atomic environment in germanic acid aqueous solutions and the solubility of germanium oxide (GeO_2, tetragonal, argutite,) in water to 500°C and 400 bar. The new data obtained were used to better constrain the stability and structure of Ge(IV) hydroxide complexes at supercritical conditions, and to provide useful comparisons of the geochemical behaviour of germanium and silicon in crustal fluids.

2. Materials and Methods

2.1. Experimental samples

Germanic acid aqueous solutions for XAFS measurements were prepared by dissolving weighted amounts of the soluble hexagonal GeO_2 polymorph (Aldrich, 99.999%) in MilliQ water at 90°C, and then were filtered through a 0.2-μm Millipore filter. The values of pH were adjusted by adding a 1M NaOH Titrisol solution and were monitored using a combination pH glass electrode. Aqueous Ge content in solutions before and after XAFS runs was analyzed by inductively coupled plasma optical emission spectroscopy (ICP-OES) and was found identical, within 1% of the value, to the initially prepared concentration. More details about solution preparation and analyses can be found in Pokrovski and Schott (1998a,b).

Argutite (GeO_2, tetragonal, rutile-like) was synthesized from commercial GeO_2 (hex) following the method of Factor and Carasso (1965) as detailed in Pokrovski and Schott (1998a). The obtained fine powder of argutite was aged for several weeks in contact with water in a titanium autoclave at 250-300°C and saturated vapor pressure (P_{sat}). Ageing runs were repeated

several times, followed each time by rapid quenching of the reactor, rinsing the solid and replacing the reacted solution with fresh water. This treatment was intended to remove ultra-fine particles and favor the formation of bigger argutite crystals (Pokrovski and Schott, 1998a). Compact crystal agglomerates and crusts of argutite larger than 1 to 2 mm in size that formed on the reactor walls were selected for XAFS dissolution experiments. Their crystallinity and crystal morphology were checked by X-ray diffraction and electronic microscopy. The good crystallinity and big size of GeO_2 crystals chosen for the experiments prevent artifacts which might otherwise lead to an overestimated solubility, due to dissolution of poorly crystallized solids or the suspension of fine and porous particles in solution on the passage of the X-ray beam during XAFS measurements.

2.2. XAFS spectra acquisition

XAFS spectra (including the X-ray absorption near edge structure region or XANES, and the extended X-ray absorption fine structure region or EXAFS) of aqueous solutions of germanic acid were collected in both transmission and fluorescence mode at the Ge K-edge (~11,104 eV) over the energy range 11,000-12,300 eV at undulator-based ID26 beamline (Gauthier et al., 1999) of the European Synchrotron Radiation Facility (ESRF, Grenoble, France). The storage ring was operated at 6 GeV with a ~200 mA current. The beam energy was selected using a Si (220) double-crystal monochromator. The beam size on the sample was focused to about 600 μm horizontal x 1000 μm vertical, thus keeping a high X-ray photon flux (~10^{13} photons/s). PIN silicon diodes were employed for measuring the intensities of incident (I0) and transmitted (I1) X-ray beam. Fluorescence spectra were collected using either a Silicon photo-diode or a 13-element Canberra detector (depending on Ge concentration).

Experimental solutions were placed in a high-pressure cell developed at the Laboratoire de Cristallographie (Grenoble). The present cell construction is based on previous designs

operating in transmission mode (Tamura et al., 1995; Soldo et al., 1998; Pokrovski et al., 2002a) and will be described in detail elsewhere (Testemale et al., *submitted*). Briefly, the apparatus consists of a poly-crystalline sapphire optical cell (Fig. 1a) which is inserted in a super-high-tension steel vessel (Fig. 1b). The vessel has a water-cooling jacket and three Be windows for X-ray passage. The cell contains a vertically oriented outer sapphire tube (internal diameter (I. D.) ~ 5 mm) with walls of ~0.2 mm in thickness and two sapphire coaxial inner rods (I. D. ~ 4.7 mm) that delimit the sample space below and above. The sample solution is placed in the gap between the two inner rods. The cell was loaded with the experimental solution under primary vacuum (~10^{-3} bar) to avoid eventual air bubbles which may create fluid inhomogeneities in the sample space. The volume of the sample space is about 0.2 cm^3. The cell has a stainless-steel flexible bellows attached to the lower end of the outer tube via a Viton seal. The bellows transmits the pressure into the tube and serves as a solution reservoir (~0.6 cm^3). The reservoir and the sample space are connected through a gap between the inner rod and the outer tube. The temperature in the sample space is maintained within ±0.2°C by Mo heating resistances and Pt-Pt/Rh thermocouples connected to a Eurotherm$^®$ temperature regulator. Temperature gradients through the sample space do not exceed 5°C at 500°C. The sample reservoir situated in the lower part far outside the heating zone (see Fig. 1a) always remains cool (<50°C when sample-space temperature is 500°C). Its position, below the sample chamber, prevents convection and therefore minimizes fluid circulation within the assembly, avoiding corrosion of the steel bellows and Viton seal by the hot fluid. The autoclave is pressurized by high-purity grade helium gas with low absorption constant for X-rays. Pressure in the sample space is always balanced with that of He gas through the bellows. Thus the sample thickness is kept constant at high T and P, and thin sapphire walls are never broken by stress. The present design permits operating up to 600°C and 1000 bar.

Two kinds of experiments were performed. The first one consisted of measuring XAFS transmission and fluorescence spectra of a germanic acid aqueous solution with an initial

concentration of 0.04 m at 400 bar from 20 to 450°C in the absence of solid phase (Experiment 1). Up to 10 scans (of ~40 min/scan data collection time) were collected and then averaged together at each temperature point. The second type of experiment was started with pure water and argutite crystals placed at the bottom of the sample space out of the X-ray beam passage (Experiment 2). The initial solid-to-solution mass ratio was about 1:6. Dissolution was studied at 400 bar from 200°C to 500°C by monitoring the Ge absorption-edge height as a function of time in transmission mode. Fluorescence spectra were also recorded, but because of lower Ge concentrations (~ 0.02 m on average) and limited beam time, they were found to be more noisy than those of the 0.04 m Ge solution (Experiment 1). As a result, quantitative EXAFS treatment was performed on both fluorescence and transmission spectra obtained in Experiment 1, whereas transmission spectra from Experiment 2 were used for measuring GeO_2 solubility.

Germanic acid aqueous solutions (0.02 - 0.09 m Ge) of slightly acid to basic pH were also recorded in both fluorescence and transmission modes at ambient temperature and pressure using fused-silica capillaries (I.D. = 3 mm, wall thickness = 0.01 mm). Germanium dioxide polymorphs of well-known crystallographic structure (quartz-like and rutile-like GeO_2; Jorgensen, 1978; Baur & Khan, 1971) which can serve as model compounds for Ge local environment, were diluted with boron nitride, carefully homogenized by grinding and shaking, pressed in pellets, and recorded similarly to the aqueous samples at ambient conditions.

2.3 Determination of solute concentration from the absorption edge height

The X-ray path length through the fluid is fixed by the geometry of the sapphire tube. As temperature increases at constant pressure, the fluid from the sample space expands into the flexible reservoir enabling changes of the fluid density. It stems from the Beer-Lambert classical X-ray absorption relation that the absorption jump over the Ge edge in such isobaric cell configuration is directly related to the amount of the absorbing species (Ge) in the fluid. Because

the solvent contribution to absorption does not vary significantly over the Ge K-edge, the amplitude of the absorption edge height at given T and P ($\Delta\mu$) can be written as

$$\Delta\mu = \Delta\sigma_{Ge}\, l\, M_{Ge}\, m_{Ge}\, d_{fluid} \tag{1}$$

where $\Delta\sigma_{Ge}$ is the change of the total absorption cross-section of Ge over its K-edge (cm^2 g^{-1}), l is the optical path length inside the cell (cm), M_{Ge} is the atomic weight of germanium (0.07259 kg mol^{-1}), m_{Ge} is the molal Ge aqueous concentration (mol kg^{-1} of solution), and d_{fluid} is the density of the aqueous solution (g cm^{-3}) at given T and P. The absorption cross-sections for Ge were taken from the recent compilation of Chantler et al. (2003). These values are in close agreement, within 2-5% below and above Ge K-edge, with older databases (e.g., Henke et al., 1993; Saloman et al., 1988). The fluid density at experimental temperature and pressure was calculated using the Pressure-Volume-Temperature (PVT) properties of pure water (Kestin et al., 1984) and assuming that the low concentrations of dissolved Ge and Al ($m_{Ge} < 0.04$, $m_{Al} < 0.0001$) do not significantly modify these properties. This assumption is supported by recent high-temperature *in situ* density measurements on aqueous solutions of germanic acid analogs, arsenious and arsenic acids, which show that density differences between a 0.1-m As solution and pure water do not exceed 2% to at least 350°C (Perfetti, 2003). Owing to the very low thermal expansion coefficient of sapphire, the X-ray path length inside the cell remains constant through the entire experiment. Because of the cylindrical shape of the sapphire tube and relatively large beam size in the horizontal plane (see Section 2.2) which makes difficult to align the beam exactly in the cell's vertical axis, the X-ray path inside the cell was calibrated at 30°C/400 bar prior to experiment using a germanic acid aqueous solution of precisely known concentration (0.0400±0.0005 m). Combining the absorption edge height determined for that sample with the value of $\Delta\sigma$ chosen above, equation (1) yielded 0.48±0.01 cm for the optical path length. This value is identical within errors to the nominal geometric inner diameter of the

tube (0.50±0.01 cm), thus further supporting the validity of equation (1). Note that such a calibration also eliminates uncertainties associated with the choice of the absorption cross-sections over Ge edge, because the measured $\Delta\mu$ values are proportional to the product of l and $\Delta\sigma$.

The presence of harmonics in the incident beam and nonlinear response of electronics and I0 and I1 detectors may further contribute to uncertainties associated with equation (1). The contribution of higher order harmonics from the Si(200) monochromator crystal at the undulator beam line ID26 equipped with two mirrors does not exceed 0.1% of the transmitted intensity in the energy and I0/I1 ranges of our experiments (Gauthier et al., 1999). The response of the I0 and I1 PIN silicon detectors is known to be linear within better than 0.1% at ID26 beamline. The overall linearity related to the whole set of electronic instruments and the present experimental setup was also checked at ambient conditions by measuring $\Delta\mu$ values of germanic acid solutions of different concentration placed in sapphire or fused silica holders with absorption coefficients similar to that of the HT-HP cell. The absorption jump amplitude was found to be linear function of Ge concentrations within ~5% in a wide range at least from 0.01 to 0.09 m.

The height of the absorption-edge step ($\Delta\mu$) in each EXAFS scan was determined using a standard normalization procedure implemented in the AUTOBK algorithm (Newville et al., 1993). A straight line is regressed to the data in the before-edge region and subtracted from the whole spectrum. Then a quadratic polynomial is regressed to the data in some region above the edge and extrapolated back to E_0 which is the energy corresponding to the maximum of the first edge derivative. The extrapolated value of the post-edge polynomial at E_0 was taken as the absorption edge height. Spectra were processed between -200 and -30 eV before the edge and between 100 and 750 eV after the edge. Notice that using such a procedure effectively avoids the uncertainties associated with variations of $\Delta\sigma$ in the near-edge region (within ~50 eV above the edge, Chantler, 2000). Moreover, an independent background removal procedure, Cromer-Liberman normalization (CLnorm, Cromer & Liberman, 1970) implemented in the Athena

software (Ravel, 2003), was used to check the validity of $\Delta\mu$ empirical determinations made by the AUTOBK algorithm. Values of $\Delta\mu$ found using both CLnorm and AUTOBK approaches were identical within errors, thus confirming the validity of estimates of atomic-like background over Ge K-edge. The uncertainty on $\Delta\mu$ determination, as estimated by changing fitted energy ranges or by comparing different scans for the same Ge solution concentration, vary from less than 1-2% of the total value for absorption steps greater than 0.2, to about 10-15% for absorption steps lower than 0.02. Considering together the uncertainties of temperature measurement ($< \pm$ 5°C; they mostly affect the fluid density calculations), those of X-ray path length, and nonlinearities in electronic instruments, it follows that equation (1) provides an absolute measure of aqueous solute concentration or mineral solubility in dilute aqueous solution (of the order of 10's millimol) with a precision better than 10% below ~300°C (where the density variations with temperature are small) and 20 to 30% at higher temperatures, for dissolved elements having K-edge energies similar to Ge at (see also Table 3).

An example of transmission XAFS scans recorded in a solubility experiment (Experiment 2) as a function of temperature at 400 bar is shown in Fig. 2. The decrease of the before-edge absorption (where germanium contribution to the absorption is small in comparison to that of water, less than ~2%) exactly follows the decrease of water density with temperature, whereas the absorption-edge height corresponds to Ge solution concentration according to equation (1).

2.4 XAFS data reduction

Data analysis was performed with the Athena and Artemis packages (Ravel, 2003) based on IFEFFIT (Newville, 2001) and AUTOBK (Newville et al., 1993) programs. Details about spectra reduction can be found in elsewhere (Pokrovski et al., 2003; Pokrovsky et al., 2004). Spectra were normalized to the absorption edge height (see Section 2.3 above), background-removed using the AUTOBK algorithm, weighted by k^n, where $1 \leq n \leq 3$, filtered over the k range

from ~1.6 to 10-17 Å^{-1} (depending on signal-to-noise ratio), and Fourier-transformed (FT) using Kaiser-Bessel window with *dk* values of 3.0, to produce radial structure functions (RSF). To obtain structural information, fits were performed in the R-space on both real and imaginary parts of one or several FT contributions (Newville, 2001). This gives the identity of the backscattering atoms, Ge-neighbor distance (R) and coordination number (N), and the Debye-Waller factor (σ^2) for a given scattering path. In addition to these structural parameters, a nonstructural parameter, ΔE, was varied in initial fits to account for its estimate made by FEFF. To diminish correlations between N and σ^2, and better account for light versus heavy neighbors and multiple scattering paths (see below), fits were performed simultaneously with k-weighting of 1, 2 and 3, and the obtained values of structural parameters were averaged. Raw EXAFS spectra were also fitted in k-space with multiple shells; they produced values of structural parameters similar to those extracted from fits of filtered signals in R-space. Theoretical backscattering amplitude and phase-shift functions for Ge-O, Ge-H, and Ge-Ge single and multiple scattering paths were computed using the FEFF 8 *ab initio* code (Ankudinov et al., 1998), using $Ge(OH)_4-(H_2O)_n$ model clusters. The amplitude reduction factor (S_o^2) used in modeling of experimental samples was fixed at 0.88±0.08 as found by fitting EXAFS spectra of germanium oxides. The influence of anharmonic disorder in determining structural parameters was checked using the cumulant expansion method (e.g., Crozier et al., 1988). The values of third- and fourth-order cumulants (c_3 and c_4) found when fitting the filtered signal for the Ge 1st coordination shell, always converged to zero within error, and, consequently, did not affect R and N values derived from fits without cumulants. The influence of possible multiple scattering (MS) events within the Ge first coordination shell was also tested using the FEFF code, assuming local T_d or O_h geometries around Ge, as found in the model compounds investigated.

3. Results

3.1 Local structure of germanium in aqueous solution

XANES spectra of the 0.04 m solution at 20 to 450°C at 400 bar and of 0.02 - 0.09 m solutions at 20°C and 1 bar (not shown) exhibit very similar edge-crest energies (11,111.0±0.5 eV) and spectral shapes. The magnitude of the white line of normalized spectra for all solutions with $m_{Ge} \leq 0.04$ m recorded in both transmission and fluorescence modes were the same, suggesting the absence of self-absorption in fluorescence mode. For the most concentrated solution (0.086 m Ge), however, minor self-absorption effects were detected in the fluorescence spectrum whose white-line magnitude was lower by about 20% in comparison to the corresponding transmission spectrum. This effect was, however, found to have no influence on EXAFS structural parameters. The shape and energy position of the spectra for all aqueous samples are similar to those of quartz-like GeO_2, thus suggesting a similar tetrahedral geometry around Ge(IV) in solution.

Normalized averaged k^2-weighted EXAFS fluorescence spectra and their Fourier Transforms of the studied 0.04-m germanic acid aqueous solutions as a function of temperature at 400 bar in Experiment 1 are presented in Fig. 3. They are pretty similar to those for 0.02 - 0.09 m solutions recorded at ambient conditions (not shown). Both low- and high-temperature spectra exhibit a 1st shell contribution from 4±0.3 oxygens at 1.75-1.76 Å (Tables 1 and 2). This is similar to the Ge-O distances and coordination numbers reported for the GeO_2 polymorph having a quartz-like structure and for numerous germanates (Jorgensen, 1978). This strongly suggests a similar tetrahedral environment for aquated Ge in solution in a wide pH (4 - 12), concentration (0.02 - 0.09 m) and temperature (20 - 450°C) range, and is consistent with the formation of Ge(IV) hydroxide complexes (note that EXAFS is not capable of seeing hydrogen atoms in most cases). At basic pH, Ge-O distance and DW factor increase significantly in comparison with those for the slightly acid solutions (Table 1), suggesting a distortion of the GeO_4 tetrahedron. This is in excellent agreement with previous solubility, potentiometric and Raman spectroscopy

studies which show that Ge aqueous speciation is dominated by the neutral $Ge(OH)_4$ complex at pH<9 and by the negative $GeO(OH)_3^-$ species at higher pH (Baes & Mesmer, 1976; Pokrovski & Schott, 1998a).

A weak 2nd contribution apparent on the RSF spectra at ~2.3 Å (not corrected for phase shift, Fig. 3) is likely to arise from multiple scattering events within the regular GeO_4 tetrahedron. This was confirmed by FEFF simulations carried out on $GeO_4(\pm H_4)\pm(H_2O)_n$ clusters. In these calculations, we adopted the S_4 symmetry for $Ge(OH)_4$ by analogy with silicic acid whose optimized geometry was modeled in many quantum chemical studies (e.g., Sefcik & Goddard, 2001; references therein). It was found that MS paths within the $[GeO_4]$ cluster such as a triangular path Ge-O1-O2, an angular path Ge-O1-Ge-O2, and a linear path Ge-O1-Ge-O1 may contribute to the EXAFS signal. Their DW factors were estimated using the equation-of-motion (EM) and recursion method (RM) models incorporated in the FEFF 8 code (Poiarkova, 1999; Poiarkova & Rehr, 1999). Both models yield close DW values for all MS paths of 0.005±0.002 $Å^2$ at 20°C which increase slightly with temperature (e.g., ~0.008 $Å^2$ at 450°C). It can be seen in Fig. 4 that the inclusion of these MS paths in the fit reasonably accounts for the 2nd shell contribution observed in Ge aqueous solutions in a wide temperature range. Possible contributions of hydrogen atoms from OH-groups or oxygens from water molecules of outer hydration shells were also tested using both qualitative wavelet analyses (Munoz et al., 2003) of our EXAFS spectra (not shown), and quantitative FEFF simulations. Both approaches demonstrated that neither hydrogens nor water molecules can account for the observed next-nearest shell signal.

3.2 Solubility of argutite in high-temperature solution and thermodynamic properties of

Ge(OH)4 (aq)

All XAFS scans for a Ge aqueous solution of 0.040-m initial concentration recorded in the X-ray cell at 400 bar from 30 to 450°C show similar absorption-edge heights at each given temperature. Germanium molal concentrations calculated from these data using equation (1) are reported in Table 3. These concentrations (~0.040±0.005 m) are identical within errors to the initial concentration at all temperatures, thus demonstrating that neither oxide precipitation nor reaction with the sapphire cell walls occurred during the experiment. The absence of Ge-oxide precipitation in the sample space at high temperature and in the colder parts of the cell from solutions supersaturated with respect to argutite (see Table 3), is consistent with the extremely slow nucleation kinetics for this mineral observed in previous work (Pokrovski & Schott, 1998a). Moreover, the good match between experimental and nominal Ge concentration within less than 10% over a wide temperature-density range implies that the uncertainties associated with the choice of the absorption cross section, estimation of atomic-like background and fluid densities are correctly accounted for at high temperature. This provides a further support for the use of a classical absorption relation (equation 1) for absolute determination of solute concentrations at extreme conditions.

The evolution of transmission XAFS spectra and Ge absorption edge height with temperature and time for consecutive scans during the argutite dissolution experiment 2 is shown in Fig. 2 and 5, respectively. It can be seen that steady state values for the absorption-edge height at 300, 350, 400, 450 and 500°C are attained within an hour after each temperature rise. Germanium steady-state concentrations derived from the edge height values using Eqn (1) are reported in Table 3 and compared with other available data in Fig. 6. Our concentrations are in excellent agreement with those previously obtained below 350°C using batch-reactor experiments with solid:solution ratios ranging from 1:3 to 1:300 and run durations from a few days to several months (Pokrovski & Schott, 1998a). Moreover, similar Ge concentrations are obtained at 400°C both on heating and cooling (see Fig. 5) demonstrating the reversibility of the dissolution reaction. These findings strongly suggest that the solid-solution equilibrium was

attained in our XAS experiment at $\geq$ 300°C. Based on the results of our XAFS analysis and previous solubility and potentiometric work (Pokrovski & Schott, 1998a; references therein) which demonstrate the formation of $Ge(OH)_4°(aq)$ at acid to neutral pH, the following reaction was adopted to describe the solubility of GeO_2 in water in a wide range of temperature and pressure:

$$GeO_2(tetr) + 2 H_2O = Ge(OH)_4°(aq) \qquad\qquad (2)$$

The equilibrium constants K(2) of reaction (2), were generated from the available data on argutite solubility obtained in the present work from 300 to 500°C at 400 bar, and in previous studies at temperatures from 25 to 350°C and pressures from P_{sat} to 1 kbar (see Fig. 6). These data show that GeO_2 solubility increases with increasing temperature up to 400°C in agreement with the previous HKF model predictions based on data obtained up to 350°C (see Pokrovski & Schott, 1998a), but decreases above 400°C, which is not predicted by the existing model. It should be emphasized that the solvation Born coefficient, ω, which accounts for the contribution of solute-solvent electrostatic interactions to the Gibbs free energy of an aqueous species in the HKF model, could not be reliably estimated in that study owing to the minor changes in this term in dense aqueous fluids below 300-350°C. In contrast, this term which is dependent on the solvent dielectric constant, becomes very sensitive to the evolution of solubility patterns and heat capacity and volume values of aqueous species in low-density solution near and above the critical point (e.g., Plyasunov & Shock, 2001). Consequently, the solubility decrease at 450 and 500°C and 400 bar measured in our study is likely due to the significant drop of both water dielectric constant and density at such conditions. These new solubility data allow a far better constraining of the HKF equation-of-state parameters for aquated Ge in supercritical fluids. The values of the heat-capacity coefficients, c_1 and c_2, and the Born parameter, ω, were refined by regression of all available log K(2) values using UT-HEL computer code (Shvarov, 1993)

consistent with the revised HKF equation of state (Tanger & Helgeson, 1988). Details about this procedure can be found in Pokrovski & Schott (1998a). In this regression, the basic thermodynamic properties ($\Delta_f G°_{298}$, $S°_{298}$, $V°_{298}$) and other HKF coefficients for $Ge(OH)_4(aq)$ were taken from Pokrovski & Schott (1998a) and kept constant because their variation was found to have negligible effect on the log K(2) values above 350°C. The refined HKF coefficients of $Ge(OH)_4(aq)$ are reported in Table 4, and the values of log K(2) calculated using these data are shown by the dashed line in Fig. 6. The Born parameter found in our study for $Ge(OH)_4°(aq)$ ($\omega \times 10^5 = 0.09$ cal/mol) is close to those of chemically similar neutral hydroxide species like $Si(OH)_4$ (0.13, Walther & Helgeson, 1977), $As(OH)_3$ (0.07, Perfetti, 2003), $B(OH)_3$ (0.06, Plyasunov & Shock, 2001), $Sb(OH)_3$ (0.05, Zotov et al., 2003) retrieved from either direct heat capacity and volume measurements or solubility data over wide temperature-pressure ranges. A positive value of ω accounts for the drop of solubility observed for argutite and quartz and the similar shape of the heat capacity patterns of neutral hydroxide species in low-density near-critical fluids (e.g., see Fig. 7).

An alternative approach to the HKF equation of state for predicting mineral solubilities and thermodynamic properties of solutes is the density model (Mesmer et al., 1988; Anderson et al., 1991; Manning, 1994) which treats the solvation contribution in terms of fluid density instead of dielectric constant. In this study, we attempted to describe GeO_2 solubility as a function of temperature using a simplest three-parameter equation (Mesmer et al., 1988):

$$\log K = A + B / T + E \cdot (\log_{10} d_{H2O}) \tag{3}$$

where A, B, and E are constants independent of temperature and pressure, T is temperature in Kelvin, and d_{H2O} is the water density (in g cm^{-3}). It can be seen in Fig. 6 (solid line) that such a simple equation fits satisfactorily the whole set of experimental data from 20 to 500°C. Although regressions involving additional terms like $[C/T^2]$, $[D/T^3]$ and/or $[F (\log d_{H2O})/T]$, which where

used to describe the water dissociation reaction (Mesmer et al., 1988) and quartz solubility (Manning, 1994) in a much wider T-P range (to 900°C and 10 kbar), yielded visually better fits, these models were less stable and exhibit both large uncertainties and strong correlations on the regression parameters, and thus judged statistically inadequate. Consequently, taking into account the relatively limited T and P range of our data, we decided to use equation (3) when deriving thermodynamic functions for reaction (2). The regression parameters A, B, and E together with their corresponding uncertainties are reported in Table 4. Differentiation of equation (3) over temperature at constant pressure yields enthalpy, entropy and isobaric heat capacity values for reaction (2) (see Mesmer et al., 1988; Anderson et al., 1991 for details). The thermodynamic properties of aqueous $Ge(OH)_4°$ were then calculated using these functions and the corresponding values for GeO_2 (tetr) and H_2O taken from Pokrovski & Schott (1998a) and Kestin et al. (1984), respectively.

It can be seen in Table 4 that the thermodynamic properties of $Ge(OH)_4$ (aq) generated in this study using both density and HKF models are similar within errors. Both equations of state account properly for the argutite solubility maximum measured in this study at 400°C (Fig. 6) and have very similar shapes outside the experimental range, exhibiting a weak solubility minimum at ~480°C (Figs. 6 & 7) and ~570°C (not shown) for the density and HKF models, respectively. The argutite solubility pattern is very similar to that documented for quartz on the basis of extensive solubility measurements (e.g., Walther & Helgeson, 1977; Manning, 1994 and references therein). At low pressures (< 500 bar), quartz solubility shows a similar well pronounced maximum near 400°C, and a weaker minimum at ~500°C. These features disappear at pressures above 1000 bar. The solubility shape predicted by the HKF and density models for both quartz and GeO_2 can be easily explained by the relative changes in solvation versus nonsolvation contributions to the aqueous species free energy as a function of dielectric constant or water density. In dense aqueous solution below 350°C (d_{H2O}>0.5-0.6 g cm^{-3}), the solvation term $E \cdot (\log_{10} d_{H2O})$ of equation (3), accounting mostly for the interactions between $Ge(OH)_4$ and

water molecules, is almost constant whereas the nonsolvation term B/T, accounting for the properties of the species itself, changes significantly with temperature owing to the increasing thermal motion. At temperatures and pressures near the critical point of water, the solvation term exhibits strong changes because of the dramatic drop of the fluid density at these conditions (Fig. 8). This explains the observed solubility decrease for most solutes near the critical point. Far above the critical point (> 450°C) at low pressures (<500 bar), the fluid density becomes very weak (<0.1 g cm^{-3}), and its evolution with temperature again very slow. As a result, the increasing thermal motion of species destabilizes the weak hydration shell and thus prevails over the solvation contribution. This explains the weak minimum of the solubility around 500°C at low pressures. At higher pressures (>600-800 bar), however, the solvation term evolves more gradually thus following the slower changes of the density as a function of temperature (Fig. 8). This renders the solubility curve smoother, without pronounced inflections (see Fig. 7). A similar reasoning can be used in the case of the HKF equation, because the dielectric constant of water, which is involved in the solvation terms of the model, exhibits a similar T-P pattern as the density (Fig. 8; Tanger & Helgeson, 1988).

Argutite solubilities predicted by both models at, for example, 700°C differ by less than 0.4 log unit at 400 bar, and ~0.25 log unit at 1000 bar, thus demonstrating the remarkable agreement of estimations at such extreme conditions made by the simplest density equation (3) involving only three adjustable parameters and by more complex HKF model which was usually considered inappropriate at densities lower than 0.3 g cm^{-3} in the absence of experimental data (e.g., Shock et al., 1992; O'Connell et al., 1996; Schulte et al., 2001). The thermodynamic parameters derived in this study allow more rigorous prediction of GeO_2 solubility and $Ge(OH)_4$ stability beyond the T-P range covered by experiments.

4. Discussion

4.1 Evolution of the local Ge(IV) structure in high-temperature crustal fluids

The EXAFS and XANES spectra of Ge(IV) aqueous solutions do not show conspicuous modifications in a wide range of temperature (20-500°C) and concentration (0.01-0.09 m), suggesting that the Ge(OH)$_4$ structure is likely to be similar in both high-density aqueous solution and low-density supercritical fluid (0.2 g cm^{-3} ≤ density ≤ 1.0 g cm^{-3} , see Tables 2 and 3). The tetrahedral geometry of the Ge(OH)$_4$ molecule shows no detectable changes, at least in the studied temperature and density range, as demonstrated by the low DW factor (~0.0015 Å^2) and the persistence with increasing temperature of the small MS contributions arising from the GeO$_4$ cluster. Similar but less symmetrical and more polar hydroxide complexes, such as As(OH)$_3$°(aq) having a pyramidal-like geometry, also show small changes of static and thermal disorder, but may in addition exhibit an increase of the O-As-O angle with increasing temperature (Testemale et al., 2004). The Ge-O distances change only very little with increasing temperature (in the limit of 0.01 Å from 20 to 450°C). This behavior is similar to that of other strongly-bound (OH)/O aqueous complexes like arsenite (As(OH)$_3$°, Pokrovski et al., 2002a; Testemale et al., 2004), modybdate (MoO$_4^{2-}$, Mosselmans et al., 1996), wolframate (WO$_4^{2-}$, Hoffmann et al., 2000), and dichromate (Cr$_2$O$_7^{2-}$, Hoffmann et al., 2001) which also show only minor changes in the metal-oxygen distances (within 0.01 Å) and DW factors in a wide temperature range. Hydrated mono- and divalent and some large trivalent cations (e.g., Rb$^+$, Ag$^+$, Sr^{2+}, Yb^{3+}, Fulton et al., 1996; Seward et al., 1996; 1999; Mayanovic et al., 2002), and aqueous neutral or charged complexes with a more ionic character (e.g., SbCl$_3$, SbCl$_4^-$, Oelkers et al., 1998; Cu^{II}Cl$_2$, Cu^{II}Cl$_3^-$, Collings et al., 2000; ZnBr$_2$, ZnBr$_4^{2-}$, Mayanovic et al., 2001; Simonet et al., 2002) demonstrate, in contrast, partial loss of the 1st water hydration shell and significant shortening of the hydration shell radius and metal-ligand bond length with increasing temperature, typically about 0.05-0.10 Å in the range 25-300°C. These changes are in agreement with the temperature evolution of solvent hydrogen bonding, and solvent-solute interactions

including such factors as dielectric saturation and solvent compressibility (e.g., Shock et al., 1992; Oelkers et al., 1998). More covalent metal complexes (e.g., $Cu^I Cl/Br$, Fulton et al., 2000; $Sn^{II}Cl_3^-$, $Sn^{II}Cl_4^{2-}$, Sherman et al., 2000), and some +2 and +3 cations (e.g., Ni^{2+}, Hoffmann et al., 1999; In^{3+}, Seward et al., 2000; Y^{3+}, Ragnarsdottir et al., 1998) exhibit only minor changes of metal-chloride and metal-oxygen distances with increasing temperature. This may be explained by the covalent character of such complexes and the strong electrostriction of the hydration shell around a small strongly charged cation (Seward et al., 2000). Thus, the constancy of the Ge-O bond length and low DW factor over the wide temperature and density range implies that due to a strong covalent character of the Ge-oxygen bonds (Pauling, 1948), the increasing thermal vibration with temperature has no significant effect on the inter-atomic distances and the structure of the Ge first atomic shell.

It should be noticed, however, that minor modifications in the symmetry, orientation or angles of Ge-O-H bonds might be induced by outer-sphere water molecules linked to the $Ge(OH)_4$ complex via hydrogen bonds. For example, molecular dynamics calculations of solvated orthosilicic acid (Rustad & Hay, 1995) indicate a diffuse hydration shell of O at ~4 Å around Si consisting of 9 to 18 water molecules. By analogy, a similar hydration shell may be expected to exist around aqueous germanium in solution. However, its detection by XAFS spectroscopy, which is very sensitive to disorder, is likely to be difficult. Despite this limitation of XAFS spectroscopy, it can be inferred from this study that changes in the structure of $Ge(OH)_4$ solvation environment with temperature are responsible for the observed germanium oxide solubility pattern which is largely controlled by the evolution of water density (or dielectric constant) at near- and supercritical temperatures. More studies that combine quantum chemical approaches and different spectroscopic methods would be necessary to quantitatively relate the solvation structures of solutes with the observed evolution of their solubilities as function of macroscopic parameters (density, dielectric constant, temperature).

4.2 Comparison with silica

The new structural and thermodynamic data obtained for the dominant $Ge(OH)_4$ species allow quantitative comparisons of the behavior of aqueous Ge and Si in high-temperature natural waters. It should be noticed that the exact structure of silicic acid in high T-P fluids is not yet firmly established. Available quartz solubility experiments in the H_2O-Ar/CO_2 systems in which water activity was varied by adding inert Ar or CO_2 (Walther & Schott, 1988; refs therein) indicate that aqueous SiO_2 is solvated by about 2 water molecules. Raman spectroscopy measurements on silicic acid at high T-P demonstrate Si-OH vibrations (Zotov & Keppler, 2002) which likely imply a $Si(OH)_4$ stoichiometry. These data are corroborated by quantum chemical calculations on silicic acid in gaseous and aqueous phase at ambient conditions (Rustad & Hay, 1995; Sefcik & Goddard, 2001). Our study on the chemically similar $Ge(OH)_4$ provides an additional support to these data, suggesting that silica is likely to form a similar tetra-hydroxide complex over wide temperature and pressure ranges. The similarity of Si- and Ge(IV)-water interaction energetics with increasing temperature is further supported by comparing the solubilities of quartz and argutite and partial molal isobaric heat capacities of silicic and germanic acids (Fig. 7). The solubility curves plotted in Fig. 7a were calculated using equation (3) generated in this study (Table 4) for GeO_2 and the density equation of Manning (1994) for SiO_2. The uncertainties for quartz solubility predictions to 600°C and 1000 bar with Manning's equation do not exceed 0.05 log units; those for argutite are expected to be within 0.3 log units (see Section 4.1). It can be seen in Fig. 7a that both minerals exhibit similar solubility patterns in water. The evolution of $Si(OH)_4$ and $Ge(OH)_4$ heat capacities obtained respectively by differentiation of Manning's relationship and equation (3) from this study is also very close (Fig. 7b). Their magnitude and evolution with temperature are typical of electrolytes (e.g., Sedlbauer et al., 2000; refs therein) and hydroxide aqueous complexes of metalloids like $B(OH)_3$

(Hnedkovsky et al., 1995), H_3PO_4 (Sharygin et al., 1997), and $H_3As^VO_4$ and $As^{III}(OH)_3$ (Perfetti, 2003).

Despite these significant similarities in the structure and thermodynamics of aqueous Ge and Si interactions with high-temperature fluids, the absolute values of germanate and silicate dissolution products and their evolution with temperature may be different. This was demonstrated by Pokrovski & Schott (1998a) who showed, for example, that the Ge/Si ratio in a fluid in equilibrium with a Ge-bearing wollastonite increases with increasing temperature. This may be responsible for the elevated values of the Ge/Si ratio measured in high-temperature fluids emanating from the oceanic ridges (e.g., Arnorsson, 1984; Froelich et al., 1985). The results of the present study support this hypothesis since they confirm the thermodynamic values of aqueous germanic acid derived in previous studies. It should be noticed however that more data on the thermodynamic properties of germanates, analogs of natural silicates, are required to model rigorously the Ge/Si ratios in high-temperature crustal fluids.

5. Concluding remarks

Solubility of argutite (GeO_2, tetr) and local atomic structure around Ge in aqueous solution were obtained to 500°C by *in situ* XAFS spectroscopy in a single series of measurements using a new X-ray optical cell. The structural parameters ($N_{Ge-O} = 4.0\pm0.3$, $R_{Ge-O} = 1.75\pm0.01$ Å, $\sigma^2 = 0.0015\pm0.0005$ Å^2) of the dominant aqueous germanium complex, $Ge(OH)_4°(aq)$, show very little changes in a wide temperature-density range (20-500°C, 1.1-0.2 g cm^{-3}). By analogy, it can be surmised that the structure of the chemically similar aqueous silicic acid, $Si(OH)_4°(aq)$, is likely to remain the same in high-temperature crustal fluids.

The evolution of argutite solubility in water as a function of temperature was found to be very similar to that of quartz, further supporting the structural similarities of Ge and Si main aqueous species. A simple 3-parameter density model was found to account for the measured

GeO$_2$ solubilities in the 20-500°C temperature range. The argutite solubility predictions beyond the experimental T-P range using the density model are in reasonable agreement with those made by the HKF equation of state refined on the basis of the new data obtained in this study. GeO$_2$ solubility pattern predicted using both models reflects changes in the solvation term (solute-solvent interactions) which closely follows the evolution of the fluid density and dielectric constant.

Despite the similarities of Ge and Si aqueous complex energetics and structure, differences in the thermodynamic properties between silicates and germanates may lead to the observed increase of Ge/Si ratio in high-temperature natural fluids as suggested by previous work. However, more thermodynamic data on these minerals and those on the structural position of Ge in natural silicates are required to rigorously use the Ge/Si fluid ratio for tracing high-temperature hydrothermal/magmatic processes.

XAFS spectroscopy can be used for direct *in situ* measurement of both solubilities and local atomic structure of metals in high-temperature crustal fluids. Our novel approach, based on a classical X-ray absorption relation coupled with knowledge of the fluid density, provides an absolute measure of metal concentration in solution. Work is currently in progress to extend such measurements on solid-liquid and liquid-vapor equilibria for other metals (e.g., Sb, Au, Cu) over magmatic-hydrothermal conditions (~few kbars, 600-800°C) using an improved X-ray cell design.

preparation. The constructive comments of the Editor, David Rickard, and two anonymous reviewers significantly improved the article's presentation.

References

Anderson, A.J., Jayanetti, S., Mayanovic, R.A., Bassett, W.A., Chou, I-M., 2002. X-ray spectroscopic inversigations of fluids in the hydrothermal diamond anvil cell: The hydration structure of aqueous La^{3+} up to 300°C and 1600 bars. Amer. Miner. 87, 262-268.

Anderson, G.M., Castet, S., Schott, J., Mesmer, R.E., 1991. The density model for estimation of thermodynamic parameters of reactions at high temperature and pressure. Geochim. Cosmochim. Acta 55, 1769-1779.

Ankudinov, A.L., Ravel, B., Rehr, J.J., Conradson, S.D., 1998. Real-space multiple-scattering calculation and interpretation of x-ray-absorption near-edge structure. Phys. Rev. B 58, 7565-7576.

Arnorsson, S., 1984. Germanium in Icelandic geothermal systems. Geochim. Cosmochim. Acta 48, 2489-2502.

Baes Jr., C.F., Mesmer, R.E., 1976. The Hydrolysis of Cations. Wiley.

Bassett, W.A., Anderson, A.J., Mayanovic, R.A., Chou, I-M., 2000. Hydrothermal diamond anvil cell for XAFS studies of first-row transition elements in aqueous solution up to supercritical conditions. Chem. Geol. 167, 1-10.

Baur, W.H., Khan, A.A., 1971. Rutile-type compounds. IV. SiO_2, GeO_2 and a comparison with other rutile-type structures. Acta Cryst. B27, 2133-2139.

Bernstein, L.R., 1985. Germanium geochemistry and mineralogy. Geochim. Cosmochim. Acta 49, 2409-2422.

Bernstein, L.R., Waychunas, G.A., 1987. Germanium crystal chemistry in hematite and goethite from the Apex Mine, Utah, and some new data on germanium in aqueous solution and in stottite. Geochim. Cosmochim. Acta 51, 623-630.

Brown, G.E., Jr., Sturchio, N.C., 2002. An overview of synchrotron radiation applications to low temperature geochemistry and environmental sciences. Rev. Miner. Geochim. 49, 1-115.

Chantler, C.T., 2000. Detailed tabulation of atomic form factors, photoelectric absorption and scattering cross section, and mass attenuation coefficients in the vicinity of absorption edges in the soft X-ray (Z=30-36, Z=60-89, E=0.1 keV-10 keV), addressing convergence issues of earlier work. J. Phys. Chem. Ref. Data 29, 597-1048.

Chantler, C.T., Olsen, K., Dragoset, R.A., Kishore, A.R., Kotochigova, S.A., Zucker, D.S., 2003. *X-Ray Form Factor, Attenuation and Scattering Tables* (version 2.0). Available online: http://physics.nist.gov/ffast. National Institute of Standards and Technology, Gaithersburg, MD.

Collings, M.D., Sherman, D.M., Ragnarsdottir, V.K., 2000. Complexation of Cu^{2+} in oxidized NaCl brines from 25 to 175°C: results from in situ EXAFS spectroscopy. Chem. Geol. 167, 65-73.

Cromer, D.T., Liberman, D., 1970. Relativistic calculations of anomalous Scattering Fractors for X-rays. J. Chem. Phys. 53, 1891-1898.

Crozier, E.D., Rehr, J.J., Ingalls, R., 1988. Amorphous and liquid systems. In X-ray Absorption: Principles, Applications, Techniques of EXAFS, SEXAFS and XANES (eds. D.C. Koningsberger, R. Prins), p. 373-442. Wiley-Interscience, New York.

Faktor, M. M., Carasso, J.I., 1965. Tetragonal germanium dioxide and equilibria in the Ge-O-H system. J. Electrochem. Soc. 112, 817-822.

Fournier, R.O., Potter, R.W., 1982. An equation correlating the solubility of quartz in water from 25° to 900°C at pressures up to 10,000 bar. Geochim. Cosmochim. Acta 46, 1969-1973.

Froelich, P.N., Hambrick, G.A., Andreae, M.O., Mortlock, R.A., Edmond, J. M., 1985. The geochemistry of inorganic germanium in natural waters. J. Geophys. Res. 90, 1122-1141.

Fulton, J.L., Pfund, D.M., Wallen, S.L., Newville, M., Stern, E.A., Ma Y., 1996. Rubidium ion hydration in ambient and supercritical water. J. Chem.. Phys. 105, 2161-2166.

Fulton, J.L., Hoffmann, M.M., Darab, J.G., 2000. An X-ray absorption fine structure study of copper(I) chloride coordination structure in water to 325°C. Chem. Phys. Lett. 330, 301-308.

Gauthier, C., Solé, A.V., Signorato, R., Goulon, J., Moguiline, E., 1999. The ESRF beamline ID26: X-ray absorption on ultra-dilute samples. J. Synchrotron Rad. 6, 164-166.

Jorgensen, J.D., 1978. Compression mechanism in α-quartz structure: SiO_2 and GeO_2. J. Appl. Phys. 49, 5473-5478.

Henke, B.L., Gullikson, E.M., Davis J.C., 1993. X-ray interactions: photoabsorption, scattering, transmission and reflection at E = 50-30,000 eV, Z = 1-92. At. Data & Nucl. Data Tables 54, 181-342.

Hnedkovsky, L., Majer, V., Wood, R.H., 1995. Volumes and heat capacities of $H_3BO_3(aq)$ at temperatures from 298.15 K to 705 K and at pressures to 35 MPa. J. Chem. Thermodynamics 27, 801-814.

Hoffmann, M.M., Darab, J.G., Fulton, J.L., 2001. An infrared and X-ray absorption study of the structure and equilibrium of chromate, bichromate, and dichromate in high-temperature aqueous solutions. J. Phys. Chem. A 105, 6876-6885.

Hoffmann, M.M., Darab, J.G., Palmer, B.J., Fulton, J.L., 1999. A transition in the Ni^{2+} complex structure from six- to four-coordinate upon formation of ion pair species in supercritical water: An X-ray absorption fine structure, near-infrared, and molecular dynamics study. J. Phys. Chem. 103, 8471-8482.

Hoffmann, M.M., Darab, J.G., Heald, S.M., Yonker, C.R., Fulton, J.L., 2000 New experimental developments for in situ XAFS studies of the chemical reactions under hydrothermal conditions. Chem. Geol. 167, 89-103.

Kestin, J., Sengers, J.V., Kamgar-Parsi, B., Levelt Sengers, J.M.H., 1984. Thermophysical properties of fluid H_2O. J. Phys. Chem. Ref. Data 13, 175-183.

Kossova, T., Dem'yanets, L., Uvarova, T., 1987. Study of germanium dioxide solubility in water at temperatures from 25 to 300°C. Russ. J. Inorg. Chem. 32, 768-772 (in Russian).

Kurtz, A.C., Derry, L.A., Chadwick, O.A., 2002. Germanium-silicon fractionation in the weathering environment. Geochim. Cosmochim. Acta 66, 1525-1537.

Manning, C.E., 1994. The solubility of quartz in H_2O in the lower crust and upper mantle. Geochim. Cosmochim. Acta 58, 4831-4839.

Mayanovic, R.A., Anderson, A.J., Bassett, W.A., Chou, I.M., 2001. Hydrogen bond breaking in aqueous solutions near the critical point. Chem. Phys. Lett. 336, 212-218.

Mayanovic, R.A., Jayanetti, S., Anderson, A.J., Bassett, W.A., Chou, I.M., 2002. The structure of Yb^{3+} aquo ion and chloro complexes in aqueous solutions at up to 500°C and 270 MPa. J. Phys. Chem. A 106, 6591-6599.

Mesmer, R.E., Marshall, W.L., Palmer, D.A., Simonson, J.M., Holmes, H.F., 1988. Thermodynamics of aqueous association and ionization reactions at high temperatures and pressures. J. Soln. Chem. 17, 699-718.

Mosselmans, J.F.W., Schofield, P.F., Charnock, J.M., Garner, C.D., Pattrick, R.A.D., Vaughan, D.J., 1996. X-ray absorption studies of metal complexes in aqueous solution at elevated temperatures. Chem. Geol. 127, 339-350.

Müller, I.H., 1926. Further studies on the allotropy of germanic oxide. Proc. Amer. Phill. Soc. 65, 183.

Murnane, R.J., Stallard, R.F., 1990. Germanium and silicon in rivers of the Orinoco drainage basin. Nature 344, 749-752.

Munoz, M., Argoul, P., Farges, F., 2003. Continuous Cauchy wavelet transform analyses of EXAFS spectra: A qualitative approach. Amer. Miner. 88, 694-700.

Newville, M., Livins, P., Yacoby, Y., Stern, E.A., Rehr, J.J., 1993. Near-edge x-ray-absorption fine structure of Pb: A comparison of theory and experiment. Phys. Rev. B47, 14126-14131.

Newville, M., 2001. IFEFFIT: interactive XAFS analysis and FEFF fitting. J. Synchrotron Rad. 8, 322-324.

O'Connell, J.P., Sharygin, A.V., Wood, R.H., 1996. Infinite dilution partial molar volumes of aqueous solutes over wide ranges of conditions. Ind. Eng. Chem. Res. 35, 2808-2812.

Oelkers, E.H., Sherman, D.M., Ragnarstottir, K.V., Collins, C., 1998. An EXAFS spectroscopic study of aqueous antimony(III)-chloride complexation at temperatures from 25 to 250°C. Chem. Geol. 151, 21-27.

Pauling, L., 1948. The Nature of the Chemical Bond. Cornell University Press.

Perfetti, E., 2003. Mesures expérimentales volumiques et calorimétriques de l'arsenic (III) et (V) en solution à 25-350°C et 0.1-29 MPa. Applications aux systèmes naturels. Master's Thesis, University Blaise Pascal, Clermont-Ferrand, France (in French).

Plyasunov, A.V., Shock, E.L., 2001. Correlation strategy for determining the parameters of the revised Helgeson-Kirkham-Flowers model for aqueous nonelectrolytes. Geochim. Cosmochim. Acta 65, 3879-3900.

Poiarkova, A.V., 1999. X-ray absorption fine structure Debye-Waller factors. Ph.D. thesis, University of Washington.

Poiarkova, A.V., Rehr, J.J., 1999. Multiple-scattering x-ray-absorption fine-structure Debye-Waller factor calculations. Phys. Rev. B 59, 948-957.

Pokrovski, G.S., Schott, J., 1998a. Thermodynamic properties of aqueous germanium (IV) hydroxide complexes from 25 to 350°C: Implications for the behavior of Ge and the Ge/Si ratio in hydrothermal fluids. Geochim. Cosmochim. Acta 62, 1631-1642.

Pokrovski, G.S., Schott, J., 1998b. Experimental study of the complexation of silicon and germanium with aqueous organic species. Implications for Ge and Si transport and the Ge/Si ratio in natural waters. Geochim. Cosmochim. Acta 62, 3413-3428.

Pokrovski, G.S., Martin, F., Hazemann, J.-L., Schott, J., 2000. An X-ray absorption fine structure spectroscopy study of germanium-organic ligand complexes in aqueous solution. Chem. Geol. 163, 151-165.

Pokrovski, G.S., Zakirov, I.V., Roux, J., Testemale, D., Hazemann, J-L., Bychkov, A.Y., Golikova, G.V., 2002a. Experimental study of arsenic speciation in vapor phase to 500°C: Implications for As transport and fractionation in low-density crustal fluids and volcanic gases. Geochim. Cosmochim. Acta 66, 3453-3480.

Pokrovski, G.S., Schott, J., Farges, F., Hazemann, J-L., 2003. Iron(III)-silica interactions in aqueous solution: Insights from X-ray absorption fine structure spectroscopy. Geochim. Cosmochim. Acta 67, 3559-3573.

Pokrovsky, O.S., Pokrovski, G.S., Schott, J., 2004. Gallium(III) adsorption on carbonates and oxides: X-ray absorption fine structure spectroscopy and surface complexation modelling. J. Colloid Interface Sci. 279, 314-325.

Ragnarsdottir, K.V., Oelkers, E.H., Sherman, D.M., Collins, C.R., 1998. Aqueous speciation of yttrium at temperatures from 25 to 340°C and P_{sat}: an in situ EXAFS study. Chem. Geol. 151, 29-39.

Ravel, B., 2003. EXAFS analysis software using IFEFFIT. *http://feff.phys.washington.edu/ ~ravel/software/exafs/*

Rustad, J.R., Hay, B.P., 1995. A molecular dymanics study of solvated orthosilicic acid and orthosilicate anion using parameterized potentials. Geochim. Cosmochim. Acta 59, 1251-1257.

Saloman, E.B., Hubbell, J.H., Scofield, J.H., 1988. X-ray attenuation cross sections for energies 100 eV to 100 keV and elements Z=1 to Z=92. At. Dat. Nucl. Dat. Tables 38, 1-197.

Sanchez-Valle, C., Martinez, I., Daniel, I., Philippot, P., Bohic, S., Simionovici, A., 2003, Dissolution of strontianite at high P-T conditions: An in-situ synchrotron X-ray fluorescence study. Amer. Miner. 88, 978-985.

Schmidt, C., Rickers, K., 2003. In-situ determination of mineral solubilities in fluids using a hydrothermal diamond-anvil cell and SR-XRF: Solubility of AgCl in water. Amer. Miner. 88, 288-292.

Schulte, M.D., Shock, E.L., Wood, R.H., 2001. The temperature dependence of the standard-state thermodynamic properties of aqueous nonelectrolytes. Geochim. Cosmochim. Acta 65, 3919-3930.

Sedlbauer, J., O'Connell, J.P., Wood, R.H., 2000. A new equation of state for correlation and prediction of standard molal thermodynamic properties of aqueous species at high temperatures and pressures. Chem. Geol. 163, 43-63.

Sefcik, J., Goddard III, W.A., 2001. Thermochemistry of silicic acid deprotonation: Comparison of gas-phase and solvated DFT calculations to experiment. Geochim. Cosmochim. Acta 65, 4435-4443.

Seward, T.M., Henderson, C.M.B., Charnock, J.M., Dobson, B.R., 1996. An X-ray absorption (EXAFS) spectroscopic study of aquated Ag in hydrothermal solutions to 350°C. Geochim. Cosmochim. Acta 60, 2273-2282.

Seward, T.M., Henderson, C.M.B., Charnock, J.M., Driesner, T., 1999. An EXAFS study of solvation and ion pairing in aqueous strontium solutions to 300°C. Geochim. Cosmochim. Acta 63, 2409-2418.

Seward, T.M., Henderson, C.M.B., Charnock, J.M., 2000. Indium(III) chloride complexing and solvation in hydrothermal solutions to 350°C: an EXAFS study. Chem. Geol. 167, 117-127.

Sharygin, A.V., Inglese, A., Sedlbauer, J., Wood, R.H., 1997. Apparent molar heat capacities of aqueous solutions of phosphoric acid and sulfur dioxide from 303 to 623 K and a pressure of 28 MPa. J. Soln. Chem. 26, 183-197.

Sherman, D.M., Ragnarsdottir, K.V., Oelkers, E.H., Collins, C.R., 2000. Speciation of tin (Sn^{2+} and Sn^{4+}) in aqueous Cl solutions from 25 to 350°C: an in situ EXAFS study. Chem. Geol. 167, 169-176.

Shock, E.L., Oelkers, E.H., Johnson, J.W., Sverjensky, D.A., Helgeson, H.C., 1992. Calculation of the thermodynamic properties of aqueous species at high pressures and temperatures: effective ionic radii, dissociation constants, and standard partial molal properties to 1000°C and 5 kbar. J. Chem. Soc. Faraday Trans. 88, 803-826.

Simonet, V., Calzavara, Y., Hazemann, J-L. Argoud, R., Geaymond, O., Raoux, D., 2002. X-ray absorption spectroscopy of ionic association in aqueous solutions of zinc bromide from normal to critical conditions. J. Chem. Phys. 117, 2771-2781.

Soldo, Y., Hazemann, JL., Aberdam, D., Inui, M., Tamura, K., Raoux, D., Pernot, E., Jal, J.F., Dupuy-Philon, J., 1998. Semiconductor-to-metal transition in fluid selenium at high pressure and temperature: An investigation using X-ray absorption spectroscopy. Phys. Rev. B 57, 258-268.

Tamura, K., Inui, M., Hosokawa, S., 1995. XAFS measurements at high temperatures and pressures. Rev. Sci. Instrum. 66, 1382-1384.

Tanger, J.C., Helgeson, H.C., 1988. Calculation of the thermodynamic and transport properties of aqueous species at high pressures and temperatures: Revised equations of state for the standard partial molal properties of ions and electrolytes. Amer. J. Sci. 288, 19-98.

Testemale, D., Argoud, R., Geaymond, O., Hazemann, J-L., *submitted*. A high pressure/high temperature cell for x-ray absorption and scattering techniques. Rev. Sci. Instruments.

Testemale, D., Hazemann, J-L., Pokrovski, G.S., Joly, Y., Roux, J., Argoud, R., Geaymond, O., 2004. Structural and electronic evolution of the $As(OH)_3$ molecule in high temperature aqueous solutions: An x-ray absorption investigation. J. Chem. Phys. 121, 8973-8982.

Walther, J.V., Helgeson, H.C, 1977.Calculation of the thermodynamic properties of aqueous silica and the solubility of quartz and its polymorphs at high pressures and temperatures. Amer. J. Sci. 277, 1315-1351.

Walther, J.V., Schott, J., 1988. The dielectric constant approach to speciation and ion pairing at high temperature and pressure. Nature 332, 635-638.

Zotov, A.V., Shikina, N.D., Akinfiev, N.N., 2003. Thermodynamic properties of the Sb(III) hydroxide complex Sb(OH)$_3$(aq) at hydrothermal conditions. Geochim. Cosmochim. Acta 67, 1821-1836.

Zotov, N., Keppler, H., 2002. Silica speciation in aqueous fluids at high pressures and temperatures. Chem. Geol. 184, 71-82.

Figure Captions

Fig. 1 Scheme of the X-ray optical cell (A) and high T-P reactor (B) used for XAFS measurements in this study.

Fig. 2 Raw XAFS transmission spectra at Ge K-edge of aqueous solutions in contact with crystalline argutite (GeO$_2$, tetr) at 400 bar and indicated temperatures (Experiment 2, see text). Each spectrum corresponds to the last scan recorded at the given temperature in the solubility experiment (see also Fig. 5). The decrease of the before-edge absorption with increasing temperature exactly follows the corresponding decrease of water density, whereas the absorption-edge height is a measure of Ge concentration in solution.

Fig. 3 Normalized k^2-weighted fluorescence EXAFS spectra of a 0.04-m germanic acid aqueous solution at 400 bar and stated temperature obtained in Experiment 1, and their corresponding Fourier Transform magnitudes (not corrected for phase shift). The vertical lines indicate the position of the 1st atomic shell around Ge composed of four oxygens in a tetrahedral arrangement, and multiple scattering contributions within the GeO$_4$ tetrahedron.

Fig. 4 Experimental spectra (solid lines) and FEFF fits (dots) for selected germanic acid solutions at conditions indicated in the Figure. EXAFS spectra weighted by k^2 (A & C) and their corresponding Fourier Transform Magnitudes (B & D).

Fig. 5 Evolution of the absorption-edge height of aqueous Ge as a function of time and temperature in an argutite dissolution run (Experiment 2). Each symbol corresponds to a XAFS scan. Arrows indicate temperature changes during the experiment; dashed lines linking the symbols at a given temperature are drawn to guide the eye. Error bars correspond to the symbol size.

Fig. 6 Logarithm of GeO$_2$ (tetr) dissolution constant (reaction 2) as a function of temperature at indicated pressures. The symbols were generated from measurements performed in this work (Table 3, Experiment 2) and previous studies. The curves represent regressions of all experimental points with the density model and the revised HKF equation of state using the parameters given in Table 4.

Fig. 7 Comparison of the solubilities of quartz (dashed line) and argutite (solid line) in pure water (A), and the partial molal heat capacities of germanic and silicic acids (B) as a function

of temperature at indicated pressures. The curves for Ge and Si were generated using respectively, equation (3) with the parameters from Table 4, and the density equation reported by Manning (1994).

Fig. 8 Water density (A) and dielectric constant (B) as a function of temperature at indicated pressures calculated according to Kestin et al. (1984). The dramatic changes in the density and dielectric constant patterns between 400 and 500°C at low pressure account for the particular solubility shapes observed for quartz and argutite (see text).

Table 1

Table 1. Structural parameters of germanium atomic environment obtained from fitting Ge K-edge EXAFS spectra of germanic acid aqueous solutions recorded at ambient temperature and pressure.

solution composition	fitted k-range $\mathring{A}^{-1}$	scatterer	N (atoms)	R (Å)	σ^2 (Å^2)	ΔE (eV)	R-factor
0.020 m H$_4$GeO$_4$ pH = 4.5	1.6-17.0	oxygen	4.3	1.753	0.0017	10.4	0.010
0.040 m H$_4$GeO$_4$ pH = 4.3	1.6-13.0	oxygen	4.1	1.750	0.0014	10.4	0.009
0.086 m H$_4$GeO$_4$ pH = 4.1	1.6-12.0	oxygen	3.8	1.749	0.0012	10.3	0.012
0.020 m H$_4$GeO$_4$ pH = 11.7	1.6-16.0	oxygen	4.1	1.761	0.0026	11.0	0.010
error of EXAFS fit			±0.3	±0.004	±30%	±1.0	

Concentrations are expressed in mol/kg of solution (m); R = germanium-oxygen mean distance, N = Ge-O coordination number, σ^2 = squared Debye-Waller factor (DW, relative to $\sigma^2 = 0$ adopted in the calculation of reference amplitude and phase functions by FEFF8); ΔE = nonstructural parameter accounting for phase shift between experimental spectrum and FEFF calculation; R-factor defines goodness of the total fit in R-space as described in FEFFIT (Newville et al., 2001). For all samples the fitted R-range was 1.1-3.0 Å (not corrected for phase shift). The following multiple scattering paths within the GeO$_4$ tetrahedron as calculated using FEFF8 (see text) were included in all fits: triangular Ge-O1-O2 (R$_{ms}$=3.19 Å, degeneracy=12); angular Ge-O1-Ge-O2 (R$_{ms}$=3.51 Å, degeneracy=12); and linear Ge-O1-Ge-O1 (R$_{ms}$=3.51 Å, degeneracy=4).

Table 2

Table 2. Structural parameters of Ge(IV) atomic environment obtained from fitting Ge K-edge EXAFS spectra of a 0.04-m germanic acid aqueous solution as a function of temperature at 400 bar (Experiment 1) [a].

T °C	fluid density g cm^{-3}	fitted k-range Å^{-1}	scatterer	N (atoms)	R (Å)	σ^2 (Å^2)	ΔE (eV)	R-factor
30	1.013	1.6-11.0	oxygen	3.8	1.748	0.0010	10.3	0.013
100	0.976	1.6-10.0	oxygen	3.8	1.751	0.0010	10.2	0.015
200	0.891	1.6-10.0	oxygen	3.9	1.749	0.0014	9.9	0.015
300	0.765	1.6-10.0	oxygen	4.1	1.746	0.0020	9.8	0.038
350	0.672	1.6-13.1	oxygen	4.2	1.749	0.0020	9.8	0.010
400	0.523	1.6-13.1	oxygen	4.2	1.752	0.0018	10.1	0.010
450	0.271	1.6-12.0	oxygen	4.0	1.749	0.0020	10.1	0.020
Error of EXAFS fit				±0.4	±0.007	±50%	±1.5	

[a] See footnotes of Table 1.

Table 3

Table 3. Germanium aqueous concentrations in equilibrium with argutite derived from the edge height of X-ray absorption spectra at Ge K-edge, and the logarithm of the equilibrium constant for reaction (2) as a function of temperature at 400 bar.

T °C	fluid density g cm^{-3}	Experiment 1 0.04m Ge(OH)$_4$-H$_2$O		Experiment 2 GeO$_2$(tetr) – H$_2$O		
		Absorption edge height	m_{Ge} mol/kg	Absorption edge height	m_{Ge} mol/kg	$\log_{10} K(2)_{T,\,400bar}$
30	1.013	0.249	0.0400 [a]	--- [b]	---	---
100	0.976	0.244	0.041±0.001	---	---	---
200	0.891	0.212	0.039±0.001	---	---	---
300	0.764	0.186	0.040±0.002	0.076	0.016±0.002	-1.80±0.07
350	0.672	0.151	0.037±0.002	0.100	0.024±0.003	-1.62±0.05
400	0.523	0.133	0.041±0.002	0.110	0.034±0.003	-1.47±0.05
450	0.271	0.072	0.043±0.005	0.048	0.029±0.004	-1.54±0.10
500	0.178	---	---	0.017	0.016±0.005	-1.80±0.15

[a] The X-ray beam optical path inside the cell was calibrated to 0.48±0.01 cm using Eqn (1), Ge initial concentration of 0.0400±0.0005mol, density of pure water at 30°C, 400 bar, and change of germanium total absorption cross-section over Ge K-edge of 174.9 cm^2 g^{-1} (Chantler et al., 2003). Uncertainties on the values of m_{Ge} and log K(2) stem mostly from those associated with the determination of the absorption edge height, X-ray path length, and water density (corresponding to a temperature variation of ±5°C in the sample chamber, see text).
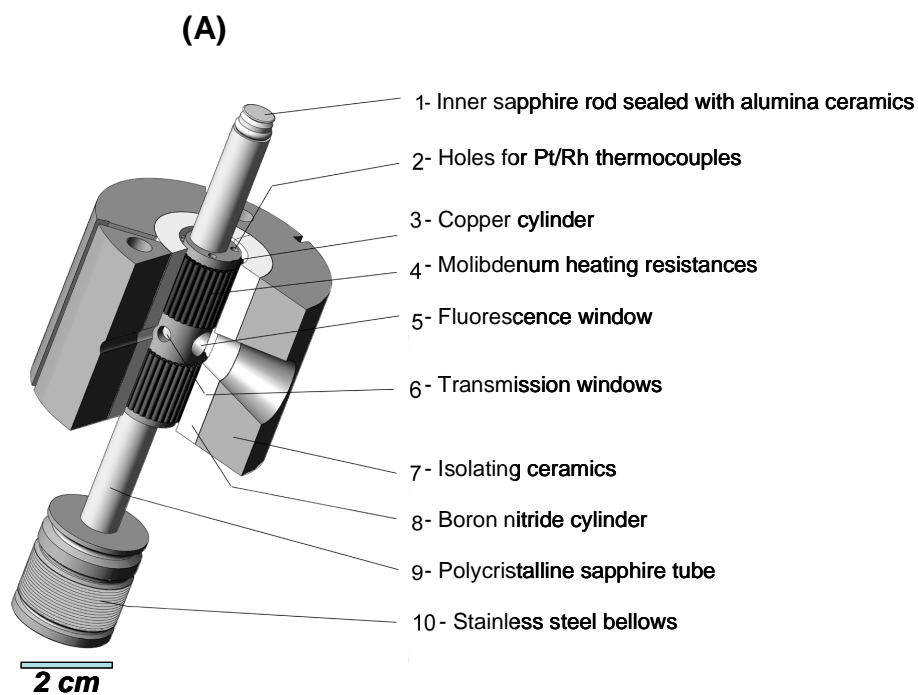[b] not measured.

Table 4

Table 4. Standard molal thermodynamic properties at 25°C and 1 bar for Ge(OH)$_4$ (aq), coefficients of equation (3), and parameters of the revised HKF model retrieved in this study.

Thermodynamic property [a]	Density equation (3)	Revised HKF equation
log K(2)	(2.02±0.17) – (2110.7±75.0) / T(K) + (1.29±0.24) * [log d$_{H2O}$ (g/cm^3)]	
Gibbs Free Energy, $\Delta_f G°$, kcal/mol	-231.1±1.0	-231.2±0.4 [b]
Enthalpy, $\Delta_f H°$, kcal/mol	-265.7±1.5	-267.0±0.9 [b]
Entropy, S°, cal/mol K	52.0±1.5	47.8±3.0 [b]
Isobaric Heat Capacity, C$_p$°, cal/mol K	45.4±2.0	50±5.0 [b]
Volume, V°, cm^3/mol	53.6±2.0	54.9 [b]
Coefficients of HKF equation of state		
a1*10, cal/(mol bar)	---	9.29 [b]
a2*10^{-2}, cal/mol	---	14.9 [b]
a3, cal K/(mol bar)	---	-0.11 [b]
a4*10^{-4}, cal K/mol	---	-3.4 [b]
c1, cal/(mol K)	---	60.0±5.0 (this study)
c2*10^{-4}, cal K/mol	---	-4.5±1.0 (this study)
ω*10^{-5}, cal/mol	---	0.09±0.01 (this study)

[a] Gibbs free energies and enthalpies of minerals and aqueous species are represented as apparent standard molal Gibbs free energies ($\Delta G°_{P,T}$) and enthalpies ($\Delta H°_{P,T}$) of formation from the elements at the subscripted pressure (P) and temperature (T) (Tanger and Helgeson, 1988). The reference states for the elements (for which $\Delta G°_{1bar,298K}$ ($\Delta H°_{1bar,298K}$) = 0) in the system Ge-O-H are elemental germanium, Ge, O$_2$, ideal gas, and H$_2$, ideal gas. The standard states for the solid phases and H$_2$O are unit activity for the pure phase at all temperatures and pressures. For aqueous species, the reference state convention corresponds to unit activity coefficient for a hypothetical one molal solution whose behavior is ideal. Aqueous species concentrations are expressed in molal units (mol/kg H$_2$O). Activity coefficients of neutral aqueous species were assumed to be unity.

[b] Pokrovski & Schott (1998a).

Figure 1

(A)

1- Inner sapphire rod sealed with alumina ceramics

2- Holes for Pt/Rh thermocouples

3- Copper cylinder

4- Molibdenum heating resistances

5- Fluorescence window

6- Transmission windows

7- Isolating ceramics

8- Boron nitride cylinder

9- Polycristalline sapphire tube

10- Stainless steel bellows

2 cm

(B)

20 cm

Figure 1. Pokrovski et al., chemge2525_revised

Figure 2
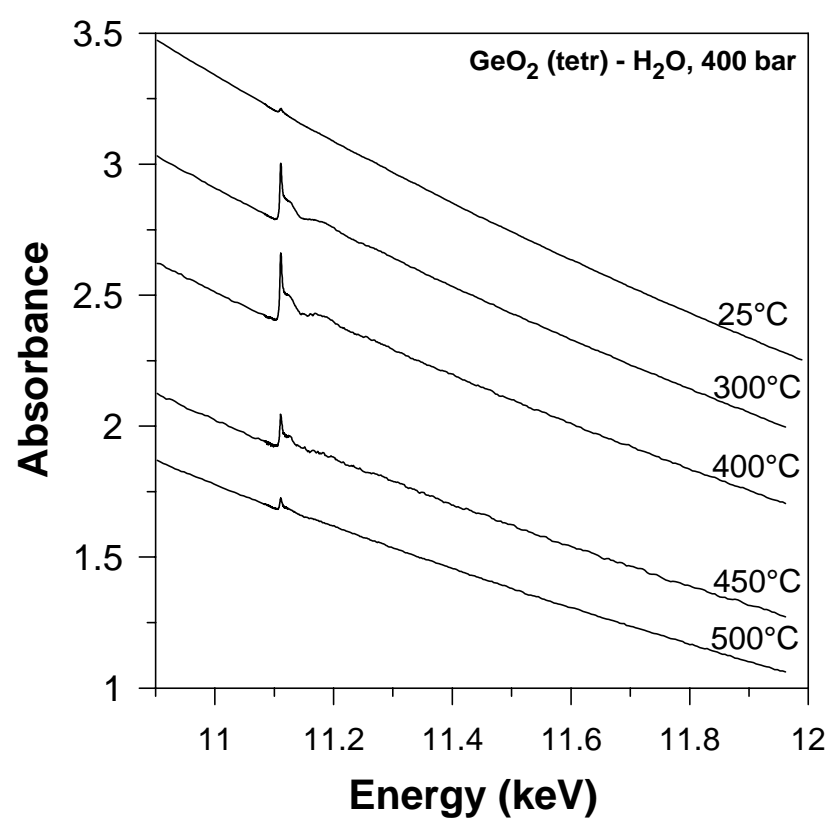
Figure 2. Pokrovski et al., chemge2525_revised

Figure 3
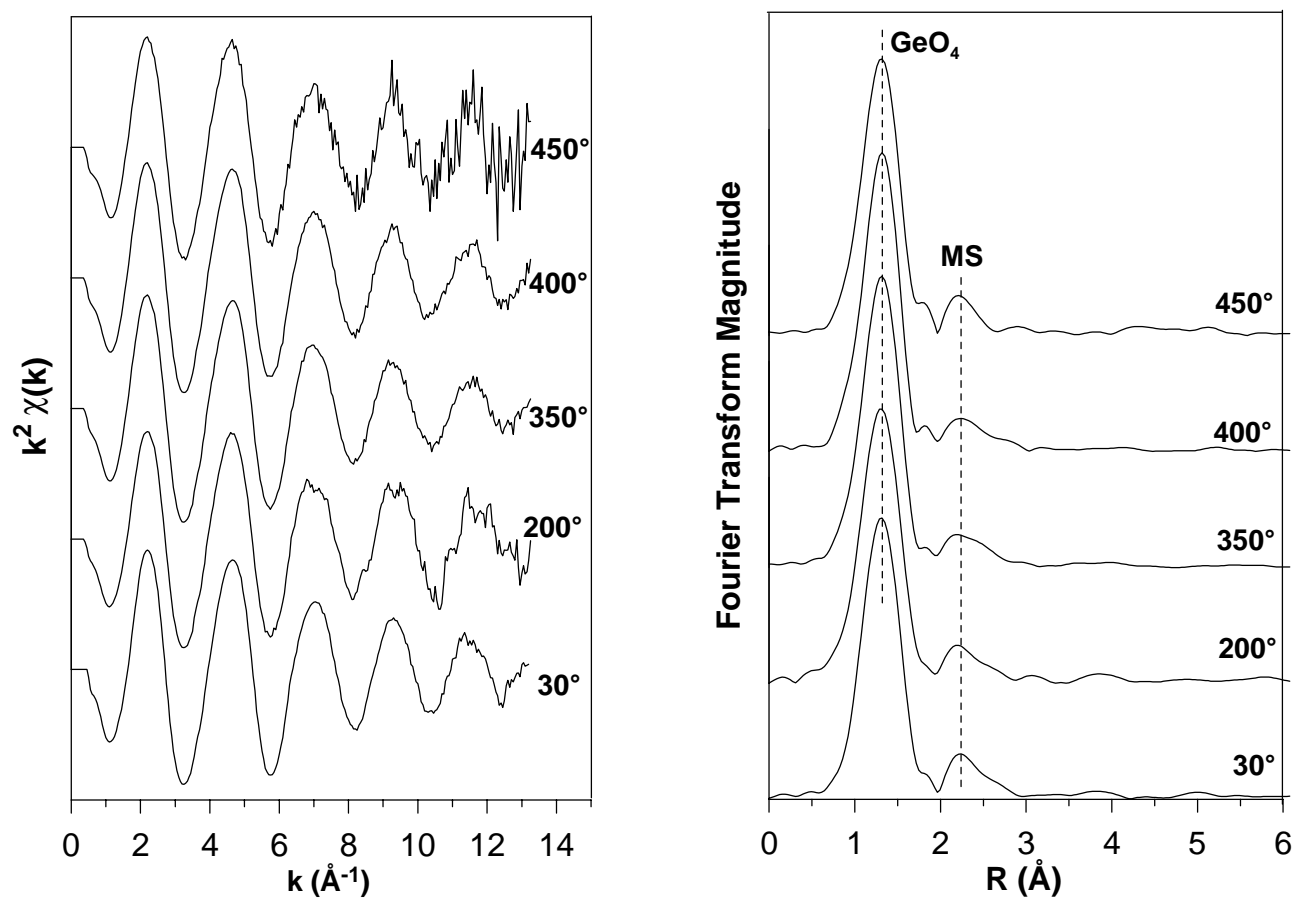
Figure 3. Pokrovski et al., chemge2525_revised

Figure 4
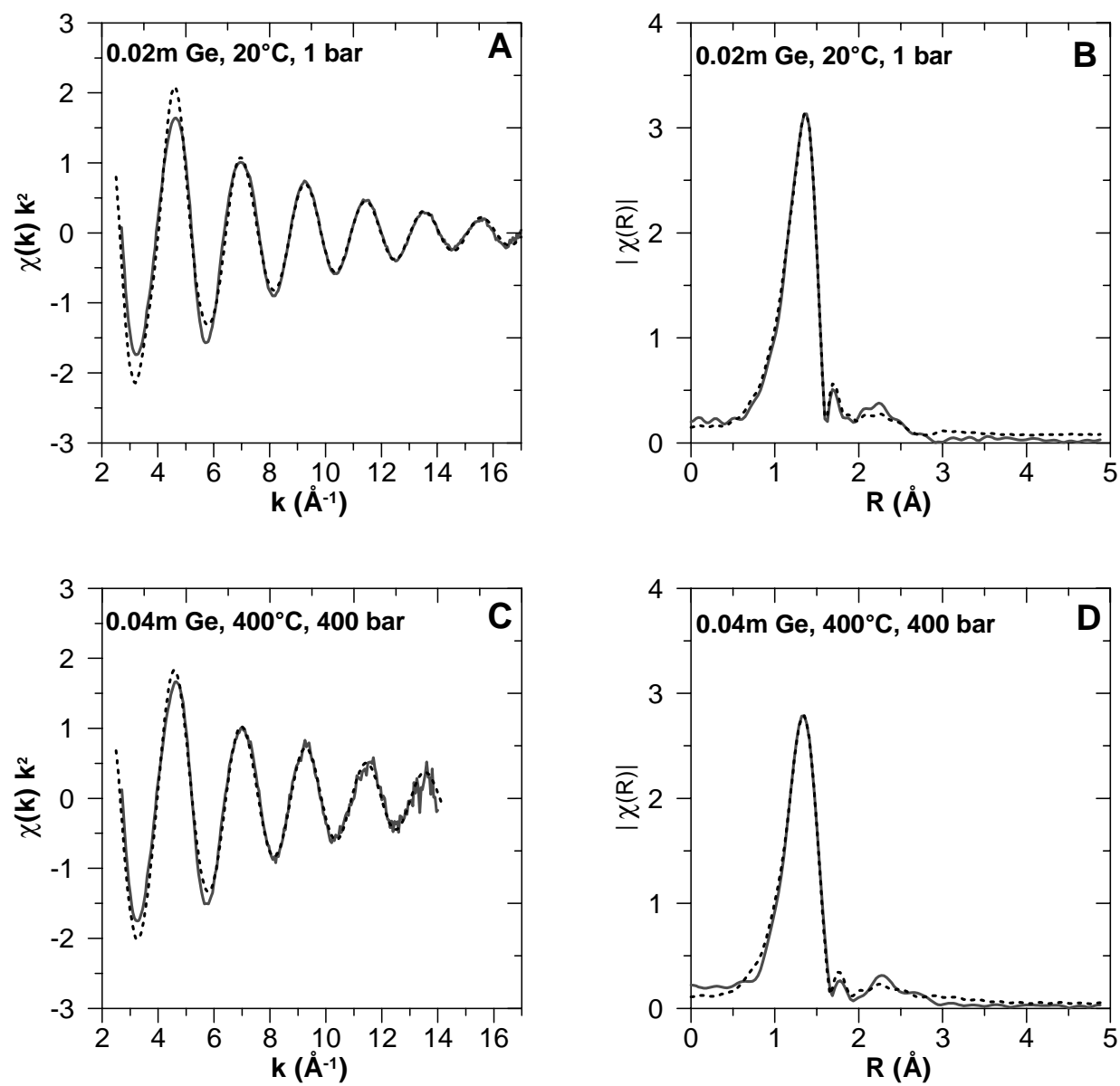
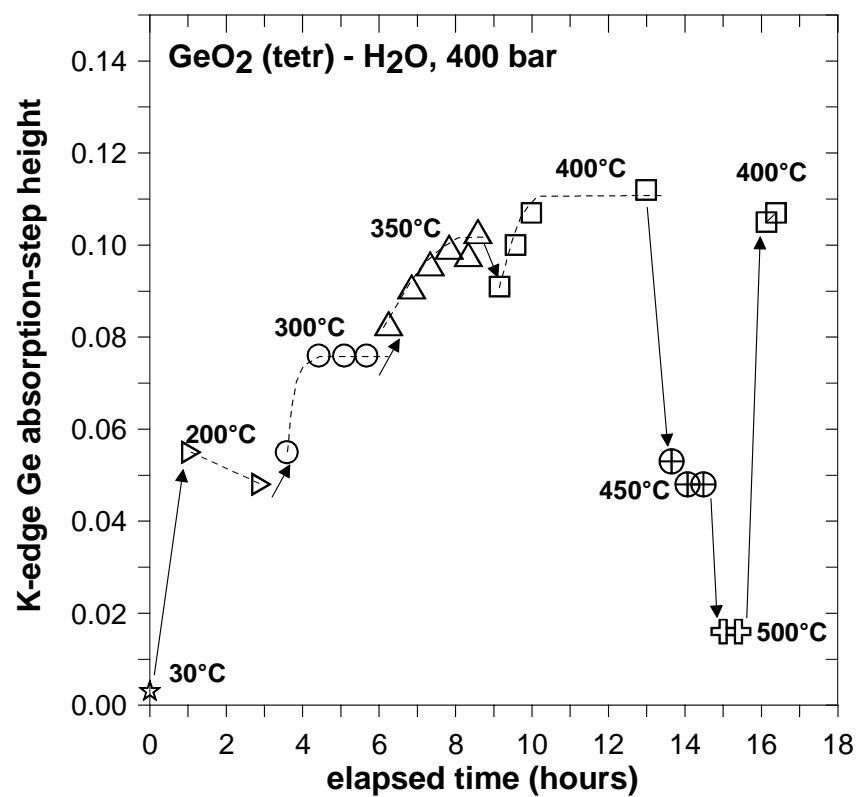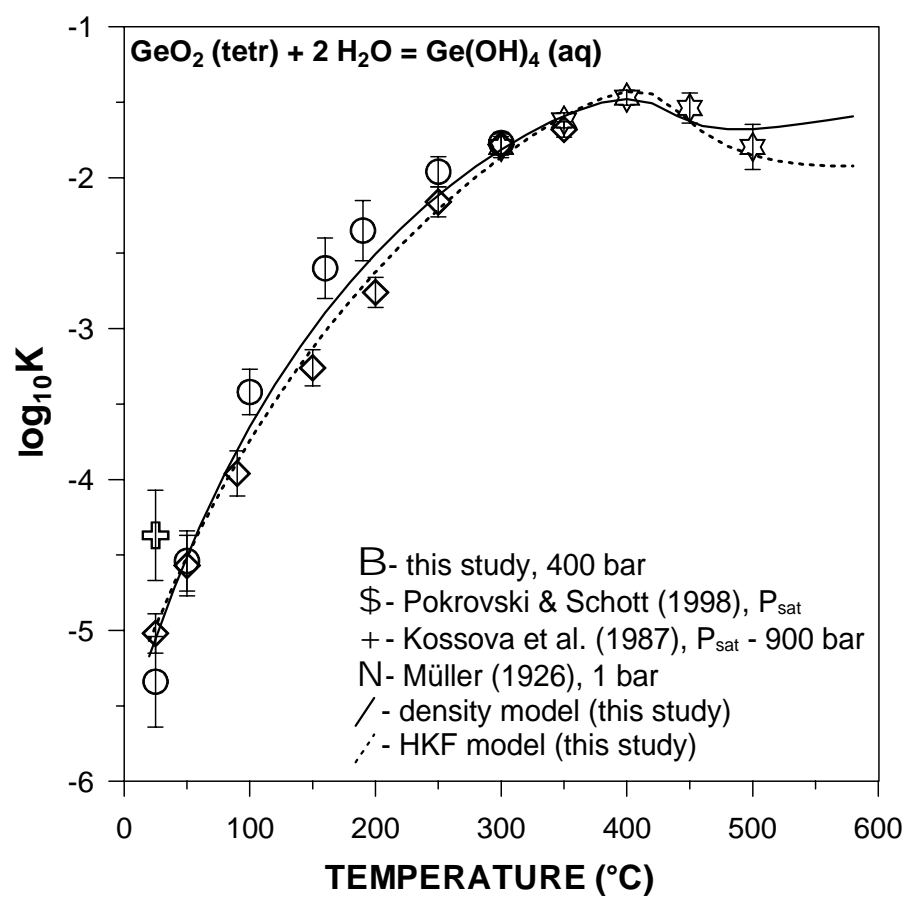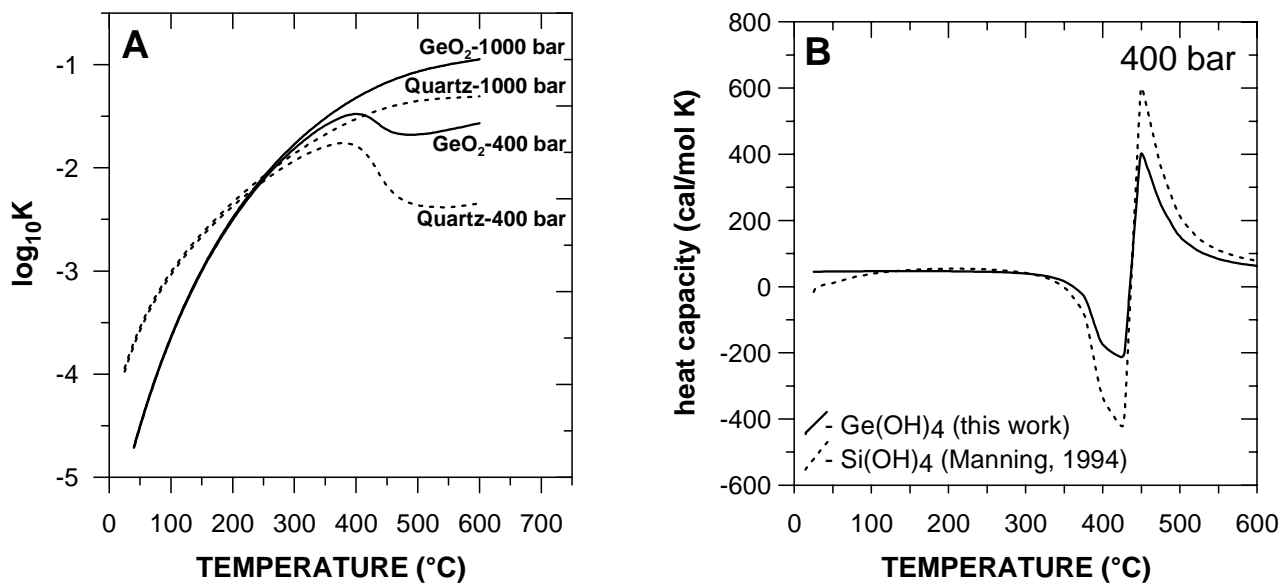**Figure 4.** Pokrovski et al., chemge2525_revised

Figure 5

Figure 5. Pokrovski et al., chemge2525_revised

Figure 6

Figure 6. Pokrovski et al., chemge2525_revised
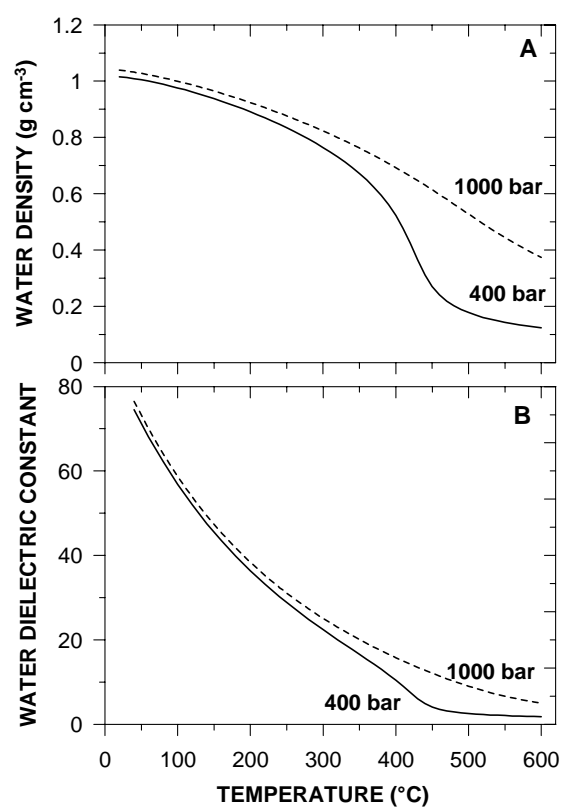
Figure 7

Figure 7. Pokrovski et al., chemge2525_revised

Figure 8

Figure 8. Pokrovski et al., chemge2525_revised